A Functional TiO₂-Coated Separator for High-Performance Li-S Batteries

Rui Wang, Jianna Deng, Jing Li, Manqin Tang, Pengyu Li, Ying Zhang*

State Key Laboratory of Environmentally Friendly Energy Materials, School of Materials Science and Engineering, Southwest University of Science and Technology, Mianyang 621010, China
*E-mail: xy13787103391@126.com

The shuttle effect of polysulfides during a cycle severely limits the further development of lithium-sulfur (Li-S) batteries. Therefore, a functional separator coated with TiO₂ was prepared. This separator chemically adsorbed polysulfides, which reduced the shuttle effect and improved the cycle stability and specific capacity during cycling. Moreover, the initial discharge capacity of the battery with a spherical TiO₂-coated separator reached 1086 mAh g^{-1} and after 100 cycles remained at 793 mAh g^{-1}, with a rate of 0.1 C. The coulombic efficiency was kept at 99%, and the capacity attenuation of each cycle was only 0.26%, which showed good cycle stability.

1. INTRODUCTION

With the development of portable electronic equipment, electric vehicles (EVs), unmanned aerial vehicles (UAVs), power grids and other new energy systems, the demand for energy storage devices with high energy density, high safety, long cycling time and low cost is increasing [1,2]. Compared with other secondary batteries, Li-S batteries have attracted more attention due to their high theoretical capacity (1675 mAh g^{-1}), high energy density (2600 Wh kg^{-1}) and relatively low cost [3-7]. However, due to a particular characteristic of the Li-S battery cathode, soluble polysulfides (Li_2S_n, $4 \leq n \leq 8$) can be produced during the cycle [8-11]. Polysulfides can diffuse through the separator to a lithium anode under the action of a concentration gradient [12,13]. This "shuttle effect" leads to the corrosion of the lithium anode and a loss of reversible active cathode material, resulting in a low sulfur utilization rate, fast capacity decay, poor rate capability and obvious self-discharge behaviour [14,17]. For this reason, many works have focused on solving the shuttle effects of polysulfides to improve the electrochemical properties of Li-S batteries.

The separator, which is situated between the S cathode and lithium anode, is one of the core components in Li-S batteries. The design of a multifunctional separator can restrain the diffusion of polysulfides across the membrane and improve the coulomb efficiency of Li-S batteries [18,19]. Based on the characteristics of charge properties, i.e., the kinetic diameter and chemical adsorption behaviour of polysulfide anions, a multifunctional separator for inhibiting the diffusion of polysulfides can be designed by an electrostatic repulsion effect [20,21], a steric hindrance effect [22] and a controlled chemical adsorption [23]. The most common strategy is to cover the separator with a layer of material that can block polysulfides on the positive side by physical adsorption or chemical bonding to achieve the purpose of inhibiting the shuttle effect. Many materials have been used to modify the separator, including montmorillonite [24], transition metal sulfides [25], carbon materials [26,27], and conductive polymers [28].

Metal oxidation is often used as a host material for S cathodes and is rarely used for separator modification. Herein, we report a simple and feasible method to prepare spherical TiO_2 by a hydrothermal method and use it to modify polypropylene (PP) separators. Due to the spherical mesoporous structure of TiO_2 and the bonding between oxygen and sulfur atoms, it shows that TiO_2 strongly adsorbs polysulfides, which can be effectively fixed on the S cathode side and inhibit the shuttle effect. Thus, the specific capacity and cycle stability of lithium-sulfur batteries are improved and show excellent electrochemical properties.

2. EXPERIMENT

2.1. Fabrication of S/VGCF composites

S / VGCF composites were prepared by filling a sealed pot with elemental sulfur (alading, AR) and vapor-grown carbon fibre (VGCF, Shenzhen, AR) at a mass ratio of 1:2 and then placed in a tubular atmosphere furnace. The composites were heated to 156 °C at a rate of 6 °C min^{-1} with a flowing Ar atmosphere, kept for 12 h and then cooled to room temperature.

2.2. Preparation of a TiO2-coated separator

Anhydrous ethanol (800 mL) was used to dissolve 0.033 mol cetylamine (HAD, structure-directing agent) and 3.20 mL KCl (0.1 mol L^{-1}). The solution was put on a magnetic stirrer, where 18.10 mL isopropanol and titanium were continuously added. After being left overnight, a gel was obtained, centrifuged and washed three times with deionized water and absolute ethyl alcohol, dried at 60 °C in a vacuum, and a TiO_2 precursor was obtained.

The TiO_2 was prepared by adding the precursor (1.6 g) to a mixture of 10 mL deionized water and 20 mL anhydrous ethanol and then dropping two drops of ammonia water (0.22 mol L^{-1}). After a uniform solution formed, it was put into an autoclave and heated in the oven for 16 hours at 160 °C. When the reaction was completed and cooled to room temperature, the product was removed,

centrifuged, washed and dried to obtain TiO_2. A schematic illustration of the fabrication of TiO_2 is shown in Fig. 1a.
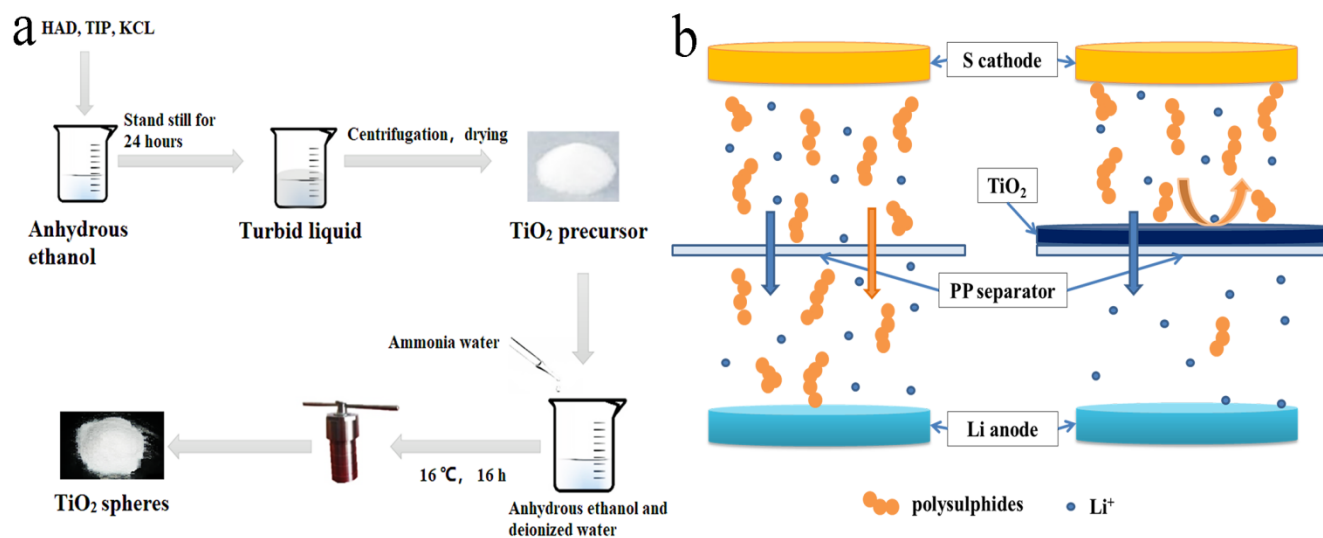

Figure 1. (a) Flow chart of the preparation of spherical TiO_2; (b) Comparison of the effect on trapping polysulfides in a Li-S battery without (left) and with a TiO_2-coated separator (right).

The prepared TiO_2, conductive carbon black (SP, Shenzhen, AR) and polyvinylidene fluoride (PVDF) were ground in an agate mortar at a mass ratio of 7:2:1 and mixed evenly by adding an appropriate amount of n-methyl-pyrrolidone (NMP). The material was coated on a separator (Celgard 2400) and dried in a vacuum at 60 °C for 24 hours.

2.3 Cell assembly and characterization

S / VGCF, SP and PVDF were mixed at a mass ratio of 7:2:1, and NMP was used as a solvent. After homogeneous mixing, the slurry was evenly coated on aluminium foil (20 µm) and dried in a vacuum at 60 °C for 24 hours. The cathode was punched into 15 mm disks. A CR2016 button battery was made using a Li anode, a TiO_2-coated separator and a S / VGCF composite cathode in an MBraun glovebox under an argon atmosphere in which the water and oxygen contents were less than 0.1 ppm. The electrolyte was 1.0 mol L^{-1} LiTFSI / DME + DOL (at a volume ratio of 1:1) and contained $LiNO_3$ (0.1 mol L^{-1}). A schematic of the TiO_2-coated separator of the battery is shown in Fig. 1b.

The crystal texture and surface morphology of TiO_2 were characterized by X-ray diffraction (XRD, D8 Advance) and scanning electron microscopy (SEM, Ultra55). The composition and structure of the samples were verified by Fourier transform infrared spectroscopy (FT-IR).

The constant current charge-discharge test was performed on a battery test system (CT2001A, LAND) at a constant current density of 0.1 C in a potential range of 1.6 - 2.8 V. The cyclic voltammetry (CV) and electrochemical impedance spectroscopy (EIS) of batteries were measured by

an electrochemical workstation (CHI660E, Shanghai). The EIS test frequency was 10^{-2} - 10^5 Hz. The CV test voltage was 1.5 - 3.0 V, and the scanning rate was 0.1 mV s^{-1}.

3. RESULTS AND DISCUSSION

Fig. 2a shows the X-ray diffraction pattern of the prepared TiO_2. The prepared TiO_2 had three characteristic peaks at 25.3°, 37.8° and 48.0°, which correlated with the peaks on the standard card (JCPDS card No. 99-0008) and indicated that anatase-type TiO_2 crystals were successfully compounded. It can be seen from Fig. 2b that the stretching vibration region of Ti-O was between 500 cm^{-1} and 700 cm^{-1}. The characteristic peak at 649.88 cm^{-1} in the figure was TiO_2. Obviously, the peak at 3429.22 cm^{-1} was the stretching vibration peak of O-H after adsorbing water from air. This proved that TiO_2 had been successfully prepared.

The prepared TiO_2 was spherical, with surface asperities and a diameter of approximately 400 nm, as shown in Fig. 2c. This spherical structure provided a large specific surface area, which was conducive to the adsorption of polysulfides. Thus, the prepared TiO_2 alleviated the shuttle effect and effectively improved the capacity of Li-S batteries.
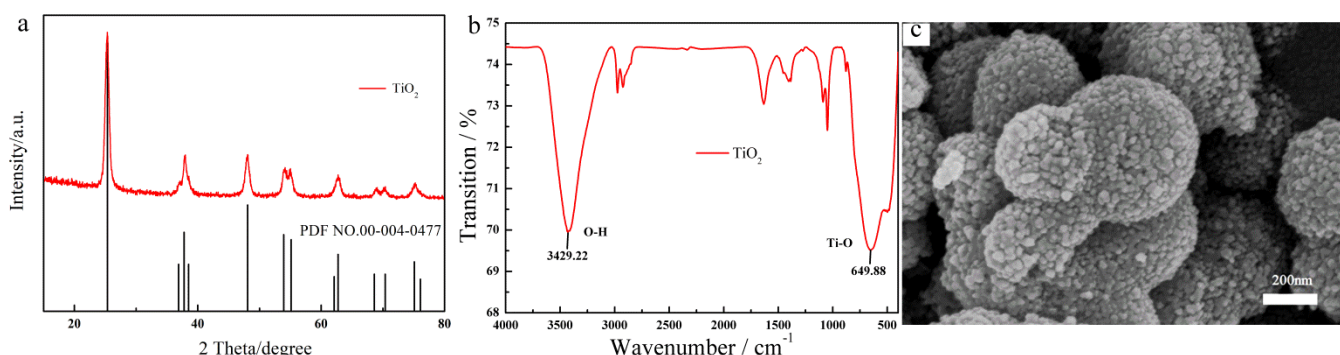

Figure 2. XRD (a), FT-IR spectra (b) and SEM pattern (c) of TiO_2.

The first charge-discharge curves for the batteries with the TiO_2 / PP functional separator and conventional PP separator are shown in Fig. 3a. It can be seen from the figure that the specific capacity of the TiO_2 / PP functional separator battery was 1086 mAh g^{-1}, which was higher than that of the modified TiO_2 / C composite separator prepared by Han et al (1060 mAh g^{-1}) [29] and 326 mAh g^{-1} more than that of a traditional PP separation battery. The reason was that the carbon accounted for a certain proportion in the TiO_2 / C composites, and the amount of polysulfide adsorbed decreased, which resulted in a difference in the first discharge capacity. At approximately 2.09 V and 2.38 V, there were several traditional platforms that reflected the S_8 reduction for soluble polysulfide lithium and the further reduction to insoluble Li_2S_2 / Li_2S, respectively [30-32]. In addition, there was a plateau at approximately 1.7 V in the discharge process of the TiO_2 / PP functional separator battery. This was a typical discharge platform of TiO_2 (TiO_2 + x Li$^+$ + x e$^-$ $\leftrightarrow$ $Li_x TiO_2$). In general, when the lithium intercalation coefficient was X = 0.5, the corresponding reversible specific capacity was 168 mAh g^{-1},

so it also contributed to part of the specific capacity[33-36]. The cycle performances of the two different separators are shown in Fig. 3b. The specific capacity of the PP separator battery decreased to 493 mAh g^{-1}, and the coulomb efficiency decreased to 75% after 100 cycles. However, the specific capacity of the TiO$_2$ / PP functional separator battery was kept at 788 mAh g^{-1}, and the coulomb efficiency was always maintained at approximately 99% under the same conditions. Compared with the work of Liu et al [37], where they modified the separator with Al$_2$O$_3$, the capacity attenuation rate of each cycle was 0.35%, while the performance of the TiO$_2$ / PP functional separator battery was better. The capacity attenuation rate of each cycle was only 0.26%, and the capacity retention rate was as high as 73%. This may be due to a stronger combination of titanium dioxide and polysulfides, which more effectively limited the shuttle effect. The excellent electrochemical performance of the TiO$_2$ / PP functional separator battery was attributed to its unique surface structure, which limited lithium polysulfide to the S cathode by chemical adsorption along with inhibited side reactions and a reduced loss of active materials.
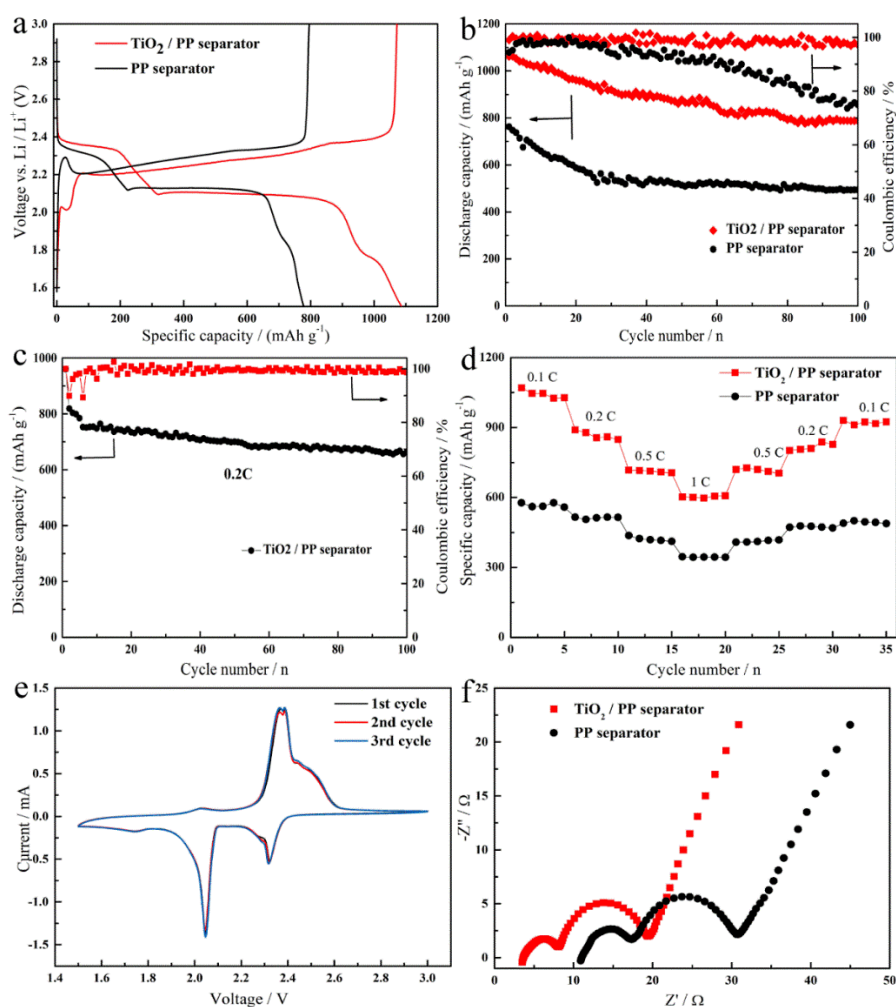

Figure 3. (a) Initial discharge-charge curves; (b) the cycle performances of the two cells at 0.1 C; (c) the cycle performance of the TiO$_2$ / PP functional separator at 0.2 C; (d) rate performance curves; (e) cyclic voltammogram profiles at a scan rate of 0.1 mV s^{-1}; (f) EIS spectra of the two cells.

Fig. 3c shows the cycle performance of the TiO_2 / PP functional separator battery during charging and discharging cycles with a high current at 0.2 C. Its first discharge specific capacity was 960 mAh g^{-1}, the capacity of the TiO_2 / PP functional separator was kept at 667 mAh g^{-1} after 100 cycles, and the capacity retention rate reached 70%. Compared with the Al_2O_3 modification of the separator by Zhang et al [38], the first capacity was 967 mAh g^{-1} and was kept at 593.4 mAh g^{-1}, with a 0.2 C current density after 50 cycles. The capacity attenuation rate of each cycle was 0.77%, which was much larger than that of the TiO_2 / PP functional separator battery (0.3%). This was consistent with the law obtained at the current density of 0.1 C. It can be seen from the two batteries that the capacity and cycle stability of the TiO_2 / PP functional separator were better than those of the PP separator in the case of heavy and low current. The rate performance of the two separators is shown in Fig. 3d. The charge-discharge performance of the two batteries was tested at current densities of 0.1 C, 0.2 C, 0.5 C and 1 C. With an increase in current density, the discharge specific capacities of the two batteries both decreased, but the discharge specific capacity of the TiO_2 / PP functional separator battery (approximately 300 mAh g^{-1}) was higher than that of the PP separator battery at the four current densities. When the density of the current increased from 0.1 C to 1 C, the discharge capacity of the TiO_2 / PP functional separator battery decreased from approximately 1000 mAh g^{-1} to 600 mAh g^{-1}. As the current density returned to its initial value, its specific capacity remained at 930 mAh g^{-1}. This indicated that the battery equipped with a TiO_2 / PP functional separator battery had good cycle stability and reversibility.

The electrochemical properties of the two batteries were measured by cyclic voltammetry and AC impedance at a scan rate of 0.1 mV s^{-1} over a voltage range of 1.7 - 2.8 V, as shown in Fig. 3e and Fig. 3f. The two reduction peaks near 2.27 V and 1.98 V were seen on cyclic voltammetry and corresponded to the reduction in S_8 to lithium polysulfides and Li_2S_2 / Li_2S. At the same time, two broad oxidation peaks were observed near 2.36 V and 2.48 V, which corresponded to the conversion of Li_2S_2 / Li_2S to lithium polysulfide and elemental sulfur. It was noteworthy that these three continuous CV curves showed almost the same shapes and positions, indicating that the batteries equipped with TiO_2 / PP functional separator batteries exhibited low polarization and excellent stability.
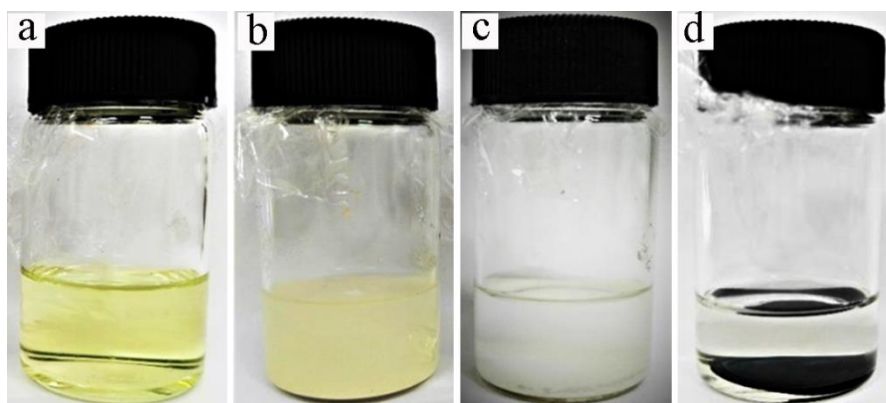

Figure 4. (a) Solution of DME : DOL (1 : 1); (b) solution just after the addition of TiO_2; (c) solution 30 min after adding TiO_2; (d) solution added to a recycled TiO_2 / PP functional separator.

The Nyquist diagram in Fig. 3e consists of a semicircle in the high- and medium-frequency region and a slant in the low-frequency region. The intercept between the curve and the cross axle represented the combined resistance (R_e), which was related to the ionic conductivity of the electrolyte, the intrinsic resistance of the active material and the contact resistance at the active material / collector interface. A constant phase element (CPE) was set to represent the double-layer capacitance, and the oblique line in the low-frequency region corresponded to the Warburg impedance. It is noteworthy that this impedance diagram was somewhat different from an ordinary impedance diagram after a cycle because it has an extra half circle. This was due to the interfacial impedance generated by the battery during the charge-discharge cycles. Compared with a traditional separator, the modified separator had smaller impedance, which was consistent with the results of the cycle performance.

To prove that TiO_2 can adsorb polysulfides, a visual verification experiment was performed, as shown in Fig. 4. The colour of the solution changed from gold to colourless (Fig. 4c) by directly adding TiO_2 powder (Fig. 4b) to the polysulfide solution, which was made by immersing the recycled S cathode in a solution of DME : DOL (1 : 1)(Fig. 1a). These results indicate that the prepared TiO_2 had a very good adsorption effect on lithium polysulfide. To further test the adsorption performance, the battery was dismantled in the glove box filled with argon after 100 cycles, and the TiO_2 / PP functional separator was removed and added to the colourless solvents DOL : DME (1 : 1)(Fig. 4d). It can be seen that the solvents were still colourless, which further illustrates that the polysulfides adsorbed on TiO_2 were not easy to desorb. The adsorption effect of TiO_2 on polysulfides was helpful for improving the cycle stability of batteries.
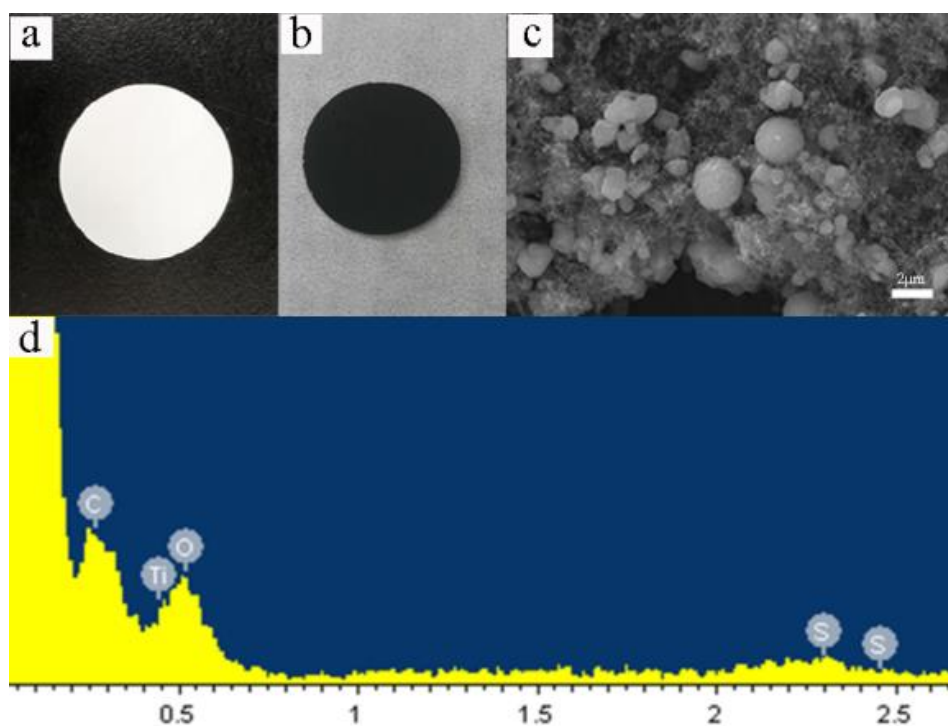

Figure 5. (a) PP separator; (b) TiO_2 / PP separator; (c) SEM and (d) EDS diagrams of the post-cyclic TiO_2 / PP separator.

To further verify the role of TiO_2 in Li-S batteries, the separator was removed after 100 cycles, as shown in Fig. 5b, and its morphology and element distribution were characterized, as shown in Fig. 5c and Fig. 5d, respectively. Combining Fig. 5c and Fig. 5d, it can be seen that TiO_2 adsorbed polysulfides, and its morphology remained unchanged after a long cycling period. These results indicated that the structure of TiO_2 was relatively stable, which helped to improve the cycle stability of the battery.

4. CONCLUSIONS

In summary, TiO_2 with a spherical structure was synthesized by a hydrothermal method and coated on a commercial separator as a functional separator for Li-S batteries. This separator was used to block the shuttle effect of batteries during cycling. As a result, after 100 cycles, the first discharge specific capacity of the TiO_2-functional separator was 1086 mAh g^{-1} and subsequently kept at 788 mAh g^{-1} with 0.1 C. The method of capturing polysulfides with a spherical porous structure of TiO_2 provides an idea for the development of Li-S batteries with high cycle stability.

References

1. X. D. Hong, J. Mei, L. Wen, Y. Y. Tong, A. J. Vasileff, L. Q. Wang, J. Liang, Z. Q. Sun and S. X. Dou, *Advanced Materials*, 31(2019) 30.
2. X. C. Lu, M. E. Bowden, V. L. Sprenkle and J. Liu, *Advanced Materials*, 27(2015) 5915-5922.
3. M. Wild, L. O'Neill, T. Zhang, R. Purkayastha, G. Minton, M. Marinescu and G. J. Offer, *Energy & Environmental Science*, 8(2015) 3477-3494.
4. A. Rosenman, E. Markevich, G. Salitra, D. Aurbach, A. Garsuch and F. F. Chesneau, *Advanced Energy Materials*, 5(2015) 21.
5. Z. W. Seh, Y. M. Sun, Q. F. Zhang and Y. Cui, *Chemical Society Reviews*, 45(2016) 5605-5634.
6. W. M. Kang, N. P. Deng, J. G. Ju, Q. X. Li, D. Y. Wu, X. M. Ma, L. Li, M. Naebe and B. W. Cheng, *Nanoscale*, 8(2016) 16541-16588.
7. R. Kumar, J. Liu, J. Y. Hwang and Y. K. Sun, *Journal of Materials Chemistry* A, 6(2018) 11582-11605.
8. G. Li, S. Wang, Y. Zhang, M. Li, Z. Chen and J. Lu, *Advanced Materials*, 30(2018) 1705590.
9. X. Zhang, D. Xie, Y. Zhong, D. Wang, J. Wu, X. Wang, X. Xia, C. Gu and J. Tu, *Chemistry – A European Journal*, 23(2017) 10610-10615.
10. S. J. Oh, J. K. Lee and W. Y. Yoon, *ChemSusChem*, 7(2014) 2562-2566.
11. S. T. Zhang, N. W. Li, H. L. Lu, J. F. Zheng, R. Zang and J. M. Cao, *Rsc Advances*, 5(2015) 50983-50988.
12. L. E. Camacho-Forero, T. W. Smith and P. B. Balbuena, *Journal of Physical Chemistry* C, 121(2017) 182-194.
13. S. M. Al-Mahmoud, J. W. Dibden, J. R. Owen, G. Denuault and N. Garcia-Araez, *Journal of Power*

Sources, 306(2016) 323-328.

14. S. Huang, R. T. Guan, S. J. Wang, M. Xiao, D. M. Han, L. Y. Sun and Y. Z. Meng, *Progress in Polymer Science*, 89(2019) 19-60.
15. Z. Xu, H. H. You, L. Zhang and Q. H. Yang, *New Carbon Materials*, 32(2017) 97-105.
16. N. P. Deng, W. M. Kang, Y. B. Liu, J. G. Ju, D. Y. Wu, L. Li, B. S. Hassan and B. W. Cheng, *Journal of Power Sources*, 331(2016) 132-155.
17. S. Rehman, K. Khan, Y. F. Zhao and Y. L. Hou, *Journal of Materials Chemistry* A, 5(2017) 3014-3038.
18. K. Yang, S. N. Zhang, D. M. Han, M. Xiao, S. J. Wang and Y. Z. Meng, *Progress in Chemistry*, 30(2018) 1942-1959.
19. Z. Wang, M. Feng, H. Sun, G. R. Li, Q. Fu, H. B. Li, J. Liu, L. Q. Sun, A. Mauger, C. M. Julien, H. M. Xie and Z. W. Chen, *Nano Energy*, 59(2019) 390-398.
20. G. L. Feng, X. H. Liu, Y. S. Wang, Z. G. Wu, C. Wu, R. Li, Y. X. Chen, X. D. Guo, B. H. Zhong and J. S. Li, *Rsc Advances*, 9(2019) 12710-12717.
21. D. J. Chen, K. C. Wen, W. Q. Lv, Z. H. Wei and W. D. He. *Physica Status Solidi-Rapid Research Letters*, 12(2018) 13.
22. R. Xu, Y. Z. Sun, Y. F. Wang, J. Q. Huang and Q. Zhang, *Chinese Chemical Letters*, 28(2017) 2235-2238.
23. J. J. Cai, Z. Y. Zhang, S. R. Yang, Y. G. Min, G. C. Yang and K. L. Zhang, *Electrochimica Acta* 9, 295(201) 900-909.
24. W. Ahn, S. N. Lim, D. U. Lee, K. B. Kim, Z. W. Chen and S. H. Yeon, *Journal of Materials Chemistry* A, 3(2015) 9461-9467.
25. K. L. Zhang, F. F. Chen, H. L. Pan, L. Wang, D. Wang, Y. Jiang, L. B. Wang and Y. T. Qian, *Inorganic Chemistry Frontiers*, 6(2019) 477-481.
26. J. Cheng, X. X. Zhang, X. F. Miao, C. W. Chen, Y. C. Liu, Y. Q. Chen, J. H. Lin, S. J. Chen, W. Wang and Y. N. Zhang, *Electrochimica Acta*, 312(2019) 358-368.
27. P. Li, J. Deng, J. Li, L. Wang and J. Guo, *Ceramics International*, 45(2019) 13219-13224.
28. H. T. Qu, J. W. Ju, B. B. Chen, N. Xue, H. P. Du, X. Q. Han, J. J. Zhang, G. J. Xu, Z. Yu, X. G. Wang and G. L. Cui, *Journal of Materials Chemistry* A, 6(2018) 23720-23729.
29. H. S. Han, S. Q. Niu, Y. Zhao, T. Z. Tan, Y. G. Zhang, *Nanoscale Res. Lett.*, 14(2019) 8.
30. R. P. Fang, S. Y. Zhao, Z. H. Sun, W. Wang, H. M. Cheng, F. Li, *Advanced Materials*, 29(2017) 25.
31. N. Jayaprakash, J. Shen, S. S. Moganty, A. Corona, L. A. Archer, *Angewandte Chemie International Edition*, 50(2011) 5904-5908.
32. V. S. Kolosnitsyn, E. V. Karaseva, *Russian Journal of Electrochemistry*, 44(2008) 506-509.
33. Y.-S. Hu, L. Kienle, Y.-G. Guo, J. Maier, *Advanced Materials*, 18(2006) 1421-1426.
34. L. Benco, J.-L. Barras, C. Daul, *Inorganic Chemistry - INORG CHEM*, 38(1998).
35. W. J. H. Borghols, M. Wagemaker, U. Lafont, E. M. Kelder, F. M. Mulder, *Chem. Mat.*, 20(2008) 2949-2955.
36. M. V. Koudriachova, N. Harrison, S. W. de Leeuw, *Physical Review B - Condensed Matter and Materials Physics*, 65(2002) 65.
37. Y. L. Liu, J. Li, M. Zeng, X. Xu, J. N. Deng, J. Q. Guo, D. Zhao, J. Z. Yang, H. R. Wang, *Int. J. Electrochem. Sci.*, 13(2018) 8189-8197.
38. Z. Y. Zhang, Y. Q. Lai, Z. A. Zhang, K. Zhang, J. E. Li, *Electrochim. Acta*, 129(2014) 55-61.